TURB'OPTY BASED OPTIMIZATION OF A SHROUDED FAN WITH CASING TREATMENT

M. Buisson[a], P. Ferrand[a], L. Soulat[a], S. Aubert[b], S. Moreau[c], C. Rambeau[b], M. Henner[d]
[a]LMFA(UMR CNRS 5509) Ecole Centrale de Lyon (France), [b]FLUOREM SA (France),
[c]GAUS Université de Sherbrooke (Canada), [d]VALEO THERMAL SYSTEMS (France)
pascal.ferrand@fluorem.com

Keywords: *optimal design, CFD, meta-model, genetic algorithm*

Abstract

Optimal design techniques recently gained a wide popularity in the industry as relatively powerful computers have become broadly available and as attractive tools such as surrogate models and evolutionary optimization went through maturation. However, when dealing with complex geometries and difficult physical phenomena to be modeled, computing costs still remain high, due to the large number of required numerical simulations feeding the traditional surrogate models. Turb'Opty™ is a meta-model which only requires a single CFD simulation at a reference configuration point, based on automatic differentiation of the discretized Reynolds-Averaged Navier-Stokes equations and high-order Taylor-series expansions. A flow database containing the derivatives of the physical variables with respect to the design variables is produced by the Turb'Opty™ parameterization tool and thoroughly explored, in the post-processing step, by a multi-parameter and multi-objective genetic algorithm coupled to the associated extrapolation tool. In this paper, post-processing of a derivative database will be depicted through a 3D study of an automotive shrouded fan with casing.

Nomenclature

x	Axial direction
Θ	Tangential direction
g	Tip clearance
h_b	Blade height
$\dot{m}_{gap}$	Leakage mass flow rate in the gap
$\Delta V_{\theta gap}$	Azimutal velocity delta between inlet and outlet of the gap
ΔPs	Static pressure delta between inlet and outlet of the fan
Ps_{in}	Mean static pressure at the fan inlet
Ps_{out}	Mean static pressure at the fan outlet
$\dot{m}$	Overall mass flow rate of the fan
r	Radius
$V_{\theta\ in}$	Mean azimutal velocity at the inlet of the fan
$V_{\theta\ out}$	Mean azimutal velocity at the outlet of the fan
ω	Rotation speed of the fan
τ	Torque of the fan
η	Static efficiency of the fan
$\boldsymbol{q}$	Vector of conservative and turbulent variables
$\boldsymbol{p}$	Vector of parameters
α_k	Stagger angle parameters
Θ_k	Leading-edge sweep parameters
$\boldsymbol{\Delta p}$	Vector of parameter variations
$\boldsymbol{F}$	Vector of total flux of discretized RANS equations
$\boldsymbol{G}$	Jacobian matrix
$\boldsymbol{R}$	First order residual
$\boldsymbol{q}^{(n)}$	Total derivative of order n of $\boldsymbol{q}$ with respect to $\boldsymbol{p}$
$\boldsymbol{G}^{(n)}$	Total derivative of order n of $\boldsymbol{G}$ with respect to $\boldsymbol{p}$
$\boldsymbol{R}^{(n)}$	Total derivative of order n of $\boldsymbol{R}$ with respect to $\boldsymbol{p}$
$\boldsymbol{b_k}$	Right-hand side of linear system
N_{pop}	Number of individuals in genetic algorithm population
N_{gen}	Number of generations achieved by genetic algorithm

1 Introduction

For modern turbomachines, the necessary clearance between casing and rotors is a major problem regarding efficient design. It is well known that this clearance is responsible for some secondary flows impinging the ”main” flow, thus generating aerodynamic losses and/or flow patterns that can trigger some instabilities such as surge and extraneous noise sources [1]. For axial compressors such as fans, the clearance is usually responsible for the biggest part of the efficiency drop. These effects may vary, depending on the size of the gap and the geometry of the machine. For the particular case of shrouded fans studied here (see Fig. 1), blades are connected together by a tip ring. This system is generally used to ensure stronger mechanical properties of the row.

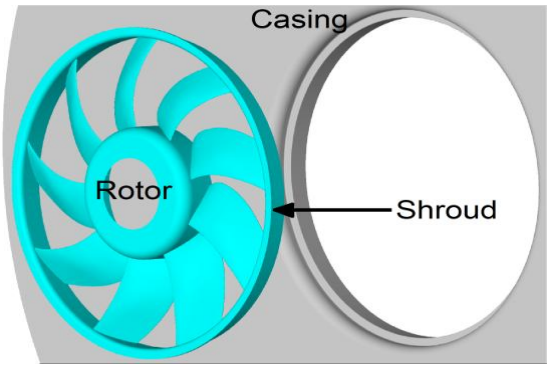

Fig. 1. 3D fan without casing treatment

Because of the pressure rise through the rotor, fluid circulates within the gap from the outlet towards the inlet of the compressor (see Fig. 2), thus reducing the overall ‘useful’ mass flow rate of the rotor and the achievable compression rate. The gap flow is also subject to a high circumferential shear between rotor and casing. As a consequence, the flow quickly accelerates in the azimutal direction, acquiring an important tangential mean velocity. This velocity is then communicated to the main flow due to viscous mixing when gap flow exits in the main stream, generating an unwanted pre-swirl in the tip region of the blades. The resulting off-design inlet flow conditions are responsible for increased aerodynamic losses.

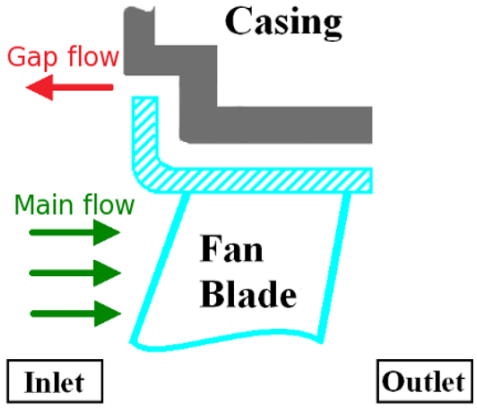

Fig. 2. Fan meridian view

In order to reduce the mass flow and the swirl of the gap flow, a new casing treament was designed and previously optimized separately from the fan using Turb’Opty^{TM} [2] (the rotor was simulated by an infinite plane with a uniform translation movement). Depending on the application, the objective and the type of turbomachine (compressor, fan, or turbine), other casing treatment techniques can be found in literature. For shrouded blades, radial fins, labyrinth seals [3][4][5], or even “bladelets” [6] are used, whereas for tip free blades, classical treatments are a circumferential grooving of the casing [7][8], slots of various shapes located above the blade, or a complex shroud shape [9] [10][11][12]. However none of these systems is designed to reduce both leakage mass flow rate and swirl. The present casing treatment consists in a helicoidal grooving of the shroud. The bent grooves are intended to provide some fluid guidance in order to limit the outlet swirl, but also to supply some blockage so as to limit the mass flow and increase the mean axial pressure gradient through the gap.

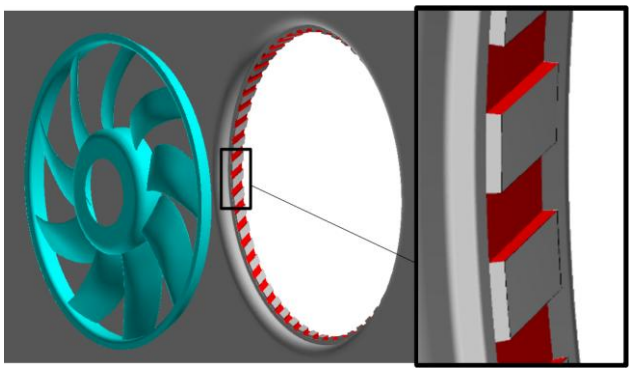

Fig. 3. 3D fan with casing treatment – Config.2

From this point of view, the higher the aerodynamic losses, the better it is. This kind of automotive low-speed cooling fan is interesting because it has an important gap due to assembly constraint (the clearance g is about a few millimeters, leading to a ratio g/h_b of 2% where h_b is the blade height). Therefore, this device is an appropriate one to prove the effectiveness of the new casing treatment.

A Reynolds-Averaged Navier-Stokes (RANS) simulation on the fan with integrated casing treatment, denoted as Config.2 (see Fig. 3), is performed using the Turb'Flow^{TM} solver [13]. Pitch periodicity is assumed in the azimutal direction as the computation is realized on a one-ninth of the complete geometry. The mesh is block-structured and is composed of 5 million nodes. A five-step Runge-Kutta second-order time scheme and a Jameson second-order spatial scheme are used. The turbulence model is the Kok's k-ω [14]. A frozen rotor model (multiple reference frames) is also used meaning that centrifugal and Coriolis forces are added into the Navier-Stokes equations for the rotating domains of the mesh. The results of such a simulation show that although the grooving performs well in terms of leakage mass flow rate $\dot{m}_{gap}$ and swirl reduction $\Delta V_{\theta gap}$ in the gap, its overall performance is disappointing compared with the one of the original fan without casing treatment, denoted as Config.1, which simulation was performed using identical numerical parameters. Indeed, Config.2 exhibits a lower static pressure difference as well as a reduced static efficiency though keeping almost identical value for the torque compared to Config.1. It should be noted that the only difference between Config.1 and Config.2 is the casing treatment; blades are identical for both configurations. Values for gap performance and for overall performances are respectively depicted in Table 1 and in Table 2.

	$\dot{m}_{gap}$ (kg/s)	$\Delta V_{\theta gap}$ (m/s)
Config. 1	0.0258	5.02
Config. 2	0.0142	3.39
Variation (%)	-45	-32.5

Table. 1. Comparison of gap performance

The explanation of such a poor overall performance is that blades were initially optimized by the fan manufacturer considering unfavorable flow conditions due to the gap flow.

	ΔPs (Pa)	τ (N.m)	η
Config. 1	198	0.499	0.641
Config.2	192	0.501	0.626
Variation (%)	-3.0	+0.4	-2.3

Table. 2. Comparison of gap performance

As a result, Config.2 is parameterized all along the radius in order to re-adapt the blades considering the enhanced tip flow conditions which are triggered by the new casing treatment. A database of derivatives as described in Section 3, whose reference is Config.2, is then produced. An optimization based on the latter derivative database is eventually achieved. The main goal of this optimization is to increase the static pressure rise in the rotor while maintaining a sufficient efficiency.

The paper is organized as follows. Section 2 presents the five parameters used to re-adapt the blades. Then, the Turb'Opty^{TM} parameterization method as well as the computation of the flow derivatives with respect to the design variables are explained in Section 3 (see [15] for a more general presentation of the method). Section 4 shows the results of the optimization which uses the latter derivative database during the evaluation process. Additional flow simulations are also presented to validate the objective values of one optimal solution.

2 Definitions of the blade shape parameters

Five geometric parameters have been considered in order to re-adapt the blade profiles with respect to the new tip flow conditions which are induced by the grooving: the hub stagger angle α_1, the mid-span stagger angle α_2, the shroud stagger angle α_3, the hub leading-edge sweep θ_1 and the mid-span leading-edge sweep θ_2.

	Δmin (°)	Ref. value(°)	Δmax(°)
α_1	-3.0	0.0	+3.0
α_2	-3.0	0.0	+3.0
α_3	-3.0	0.0	+3.0
θ_1	-3.0	0.0	+3.0
θ_2	-3.0	0.0	+3.0

Table. 3. 3D fan parameter ranges

Their respective ranges are listed in Table 3. A variation of any of these parameters triggers a mesh deformation which is calculated using analytical functions trough Turb'Mesh^{TM}. This mesh deformation is taken into account during the computation of the derivative database.
As far as the stagger angles are concerned (see Fig. 4), moving towards the red dotted line means $\Delta\alpha_k$ takes a negative value and creates a more staggered profile, whereas moving towards the blue dotted line means $\Delta\alpha_k$ takes a positive value and creates a less staggered profile. These three design variables enable the evolution of the stagger angle to be quadratic from hub to shroud.

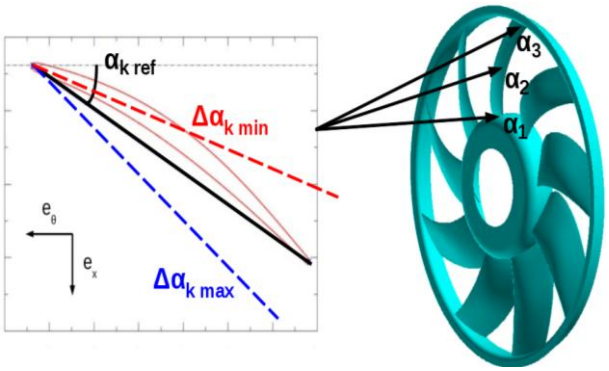

Fig. 4. Parameterized stagger angles α_k (k=1,2,3)

As far as the leading-edge sweeps are concerned (see Fig. 5 and Fig. 6), moving towards the red dotted line means $\Delta\theta_k$ takes a negative value and creates a more swept blade, whereas moving towards the blue dotted line means $\Delta\theta_k$ takes a positive value and creates a less swept blade.
It should be pointed out that the shroud remains fixed when changing the value of θ_1 and that both hub and shroud remain fixed when changing the value of θ_2. These two design variables enable the evolution of the leading-edge sweep to be quadratic from hub to shroud.

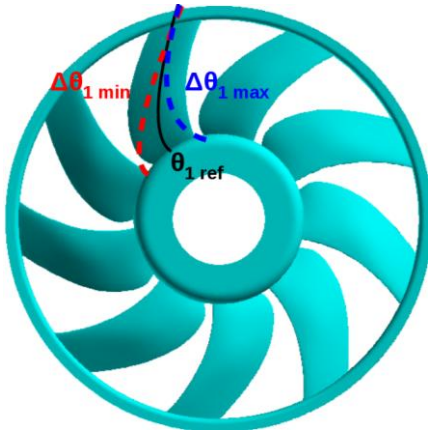

Fig. 5. Parameterized hub forward sweep θ_1

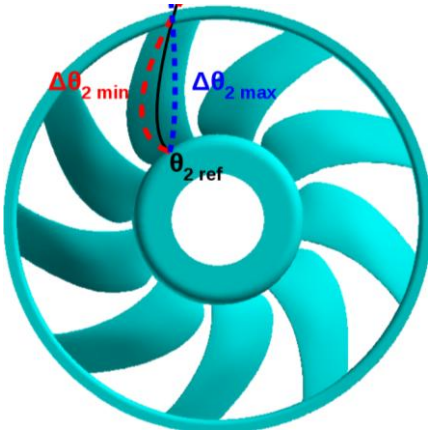

Fig. 6. Parameterized hub forward sweep θ_2

3 Computing the Derivative Database

The first step of the Turb'Opty^{TM} parameterization method is to perform a steady RANS simulation on a reference configuration using a CFD solver. In the present paper, the reference configuration is Config.2 and the Turb'Flow^{TM} software is used as mentioned earlier in Section 1. When convergence is reached, the discretized steady RANS equations can be written in the following symbolic form:

$$\mathbf{F}(\mathbf{q}(\mathbf{p}),\mathbf{p}) = \mathbf{0} \qquad (1)$$

With $\boldsymbol{F}$ the flux vector expressing mass, momentum and energy conservation with respect to $\boldsymbol{q}$ which contains the conservative variables (ρ, $\rho\boldsymbol{V}$, ρE) and the transport of turbulent variables ρk and $\rho\omega$. $\boldsymbol{F}$ includes both convective and viscous fluxes.

Once discretized, the steady RANS equations can be differentiated with respect to the design variables ***p*** using automatic differentiation [16]. The first-order automatic differentiation of equation 1 gives:

$$\frac{\partial \mathbf{F}}{\partial \mathbf{q}}(\mathbf{q},\mathbf{p}).\mathbf{q}^{(1)}.\Delta\mathbf{p} = -\frac{\partial \mathbf{F}}{\partial \mathbf{p}}(\mathbf{q},\mathbf{p}).\Delta\mathbf{p} \qquad (2)$$

where $\boldsymbol{q}^{(1)}$ is the desired first-order derivative of ***q*** with respect to the parameters vector ***p***. Denoting $\mathbf{G} = \partial\mathbf{F}/\partial\mathbf{q}$ the Jacobian matrix and ***R***(***q***, ***p***, Δ***p***) the right hand side of equation (2), the high-order derivatives $\boldsymbol{q}^{(n)}$ of ***q*** with respect to ***p*** are then recursively built by subsequent automatic differentiations of equation (2):

$$\mathbf{G}.\mathbf{q}^{(1)}.\Delta\mathbf{p} = \mathbf{R} \qquad (3)$$

$$\mathbf{G}.\mathbf{q}^{(2)}.\Delta\mathbf{p} = \mathbf{R}^{(1)} - \mathbf{G}^{(1)}.\mathbf{q}^{(1)}.\Delta\mathbf{p} \qquad (4)$$

$$\ldots \qquad \ldots \qquad \ldots$$

$$\mathbf{G}.\mathbf{q}^{(n)}.\Delta\mathbf{p} = \mathbf{R}^{(n-1)} - \sum_{i=1}^{i=n-1} C_{n-1}^{i}\mathbf{G}^{(i)}.\mathbf{q}^{(n-i)}.\Delta\mathbf{p} \qquad (5)$$

Once the derivatives have been computed and stored, the flow field corresponding to any modified parameters vector ***p***+Δ***p*** can be approximated by a multi-parameters high-order Taylor-series expansion:

$$\mathbf{q}(\mathbf{p}+\Delta\mathbf{p}) = \mathbf{q}(\mathbf{p}) + \mathbf{q}^{(1)}.\Delta\mathbf{p} + \ldots + \frac{\mathbf{q}^{(n)}}{n!}\Delta\mathbf{p}^{n} + O(\Delta\mathbf{p}^{n+1}) \qquad (6)$$

In equation 6, the truncation error is of the order of magnitude of $\Delta\boldsymbol{p}^{(n+1)}$ and ***q***(***p***+Δ***p***) satisfies the equilibrium condition to the n^{th}-order approximation:

$$\mathbf{F}(\mathbf{q}(\mathbf{p}+\Delta\mathbf{p}),\mathbf{p}+\Delta\mathbf{p}) = \mathbf{0} + o(\Delta\mathbf{p}^{n}) \qquad (7)$$

For each order *k* of the derivative, a linear system of the form $\boldsymbol{G}\boldsymbol{q}^{(k)} = \boldsymbol{b}_k$ is solved. ***G*** is always the same Jacobian matrix; only the right-hand side $\boldsymbol{b}_k$ changes and is deduced from the order *k-1*.

The resolution of the linear system (see [17] for an overview of the methods) is based on a Krylov iterative method preconditioned with an additive Schwarz domain decomposition technique. An incomplete LU factorization is used to approximate the sub-domain operator.

As five parameters are used, the whole derivative database contains, five first-order derivatives, five second-order derivatives and ten second-order cross-derivatives for a total number of twenty derivatives. As an example, the residual's l2 norm of the iterative method is plotted in Figure 7 when computing the second-order derivatives of the flow variables with respect to the hub stagger angle α_1.

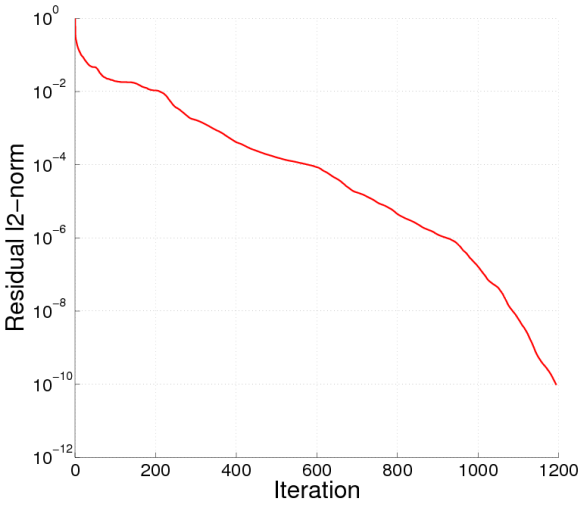

Fig. 7. Convergence of the Krylov iterative method

It should be noted that the computation of the whole derivative database is performed on the same reference geometry Config.2 but with a coarser grid composed of 500 000 nodes. This is due to memory constraints and to the available computing resources. Moreover, turbulence is frozen during the computation. Some previous derivative computations including turbulence in the linear system have shown a deterioration of the Jacobian matrix pre-conditioning leading to unconverged results. In this paper, the derivatives of the turbulent variables ρk and $\rho\omega$ with respect to the parameters are equal to zero meaning that the turbulence level for any extrapolated flow field is the same as the one of the reference configuration (frozen turbulence).

As the Jacobian matrix is the same for each derivative computation, its pre-conditioning is performed only once. The elapsed time for pre-conditioning is 3.5 hours. The mean elapsed time for solving each linear system (i.e. computing each derivative) is 3.5 hours. Therefore, the whole derivative database containing 20 derivatives is obtained in about 3.5+20*3.5=73.5 hours. 12 cores from 3 Intel Xeon X5550 processors are used and these processors are distributed over 3 nodes of 72Go of memory each. Global memory usage is roughly 120Go.

4 Multi-parameter Multi-objective Optimization

In the post-processing step, the whole flow field can be extrapolated almost instantaneously (read/write procedure) for any variation of the parameters. This means that any optimization criterion based on the extrapolated flow variables can be evaluated thereafter. The extrapolation tool is coupled to Non-dominated Sorting Genetic Algorithm 2 (NSGA2) [19]. In the present paper, extrapolation is of second order including the cross derivatives. The same three objectives as in Section 1 are used and vary according to the five parameters described in Section 2. For sake of clarity, definitions of the objectives are recalled:

- maximization of static pressure difference:

$$\Delta Ps = Ps_{out} - Ps_{in}$$

- minimization of the torque:

$$\tau = \dot{m}.(r.V_{\theta\,out} - r.V_{\theta\,in})$$

- maximization of the static efficiency:

$$\eta = (\Delta Ps \,.\, \dot{m}) \,/\, (\tau \,.\, \Omega)$$

NSGA2 is run with a population of N_{pop} = 500 individuals evolving during N_{gen} = 100 generations in order to thoroughly explore the parameter space. This corresponds to 50 000 calls of the extrapolation tool. This post-processing method of the derivative database takes approximately 5 hours on this 500 000 node mesh, using 1 core of an Intel Xeon X5460 processor.

It should be noted that changing one or more objectives for the optimization process does not involve computing once again the whole derivative database. Only the routine that evaluates the criterion is modified. When using another meta-modeling technique that requires numerous flow simulations (see [18] for a review of the different techniques), changing a criterion involves building once again the meta-model.

Figures 8, 9 and 10 show in blue circles the three projected views of the obtained Pareto optimal population also called Pareto surface. Objective values of the reference configuration Config.2 are depicted as a black square and those of two Pareto optimal solutions of special interest, Config.3 and Config.4, are respectively represented as a red downward-pointing triangle and a green upward-pointing triangle. Their respective $\Delta \boldsymbol{p}$ values (with respect to the reference configuration) are listed in Table 4.

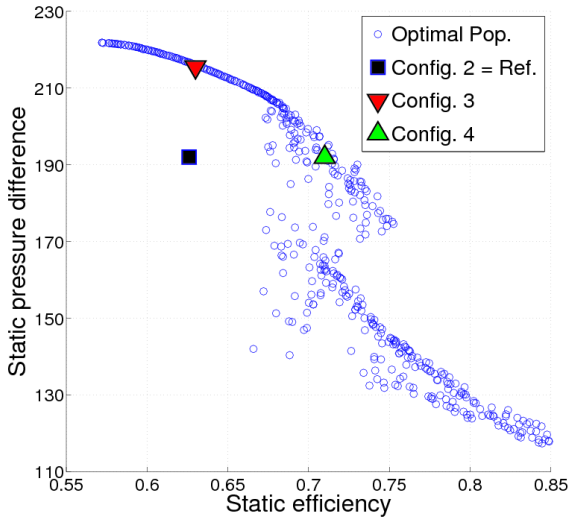

Fig. 8. (η, ΔPs) projection of the Pareto surface

On the one hand, Config.3 has been chosen because it maintains the same level of static efficiency η while increasing the static pressure difference ΔPs. The torque τ being negatively correlated to the static pressure difference, this

automatically prompts a deterioration of this latter objective.

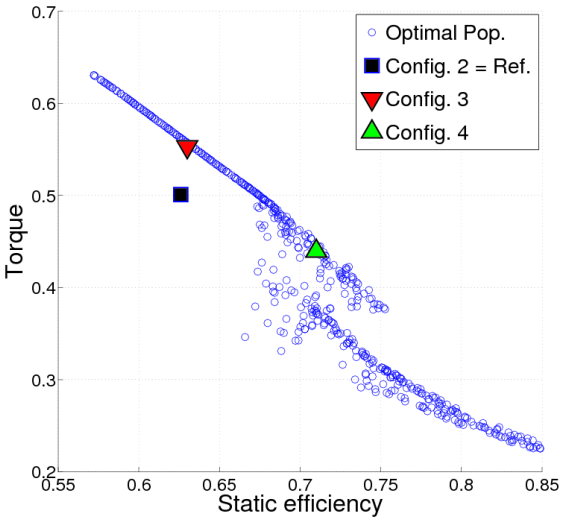

Fig. 9. (η, τ) projection of the Pareto surface

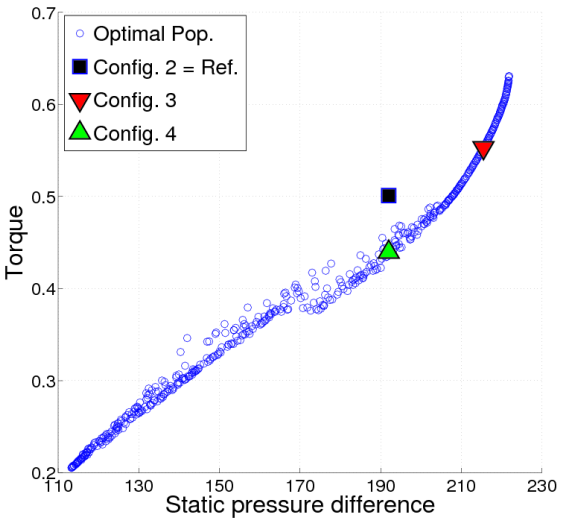

Fig. 10. (ΔP, τ) projection of the Pareto surface

On the other hand, Config.4 has been considered because it keeps the same level of static pressure difference while enhancing both the static efficiency and the torque. Table 5 sums up the overall performance for Config.2, Config.3 and Config.4. Table 6 compares the gap performances between each configuration.
As the pressure rise in the rotor is identical between Config.4 and the reference configuration, few differences can be observed regarding the mass flow rate $\dot{m}_{gap}$ in the gap between these two configurations.

	Config.3	Config.4
α_1	-3.0°	-2.0°
α_2	2.0°	-1.0°
α_3	2.0°	2.0°
θ_1	-2.2°	-2.5°
θ_2	3.0°	3.0°

Table 4. **Δp** values for the two chosen optima

	ΔPs (Pa)	τ (N.m)	η
Config.2(Turb'Flow)	192	0.501	0.626
Config.3 (Turb'Opty)	214	0.533	0.630
Config.4 (Turb'Opty)	192	0.440	0.710

Table 5. Comparison of overall performance

	$\dot{m}_{gap}$ (kg/s)	$\Delta V_{\theta gap}$ (m/s)
Config.2(Turb'Flow)	0.0142	3.39
Config.3 (Turb'Opty)	0.0161	1.60
Config.4 (Turb'Opty)	0.0150	0.80

Table 6. Comparison of gap performance

However, Config.4 enables to reduce the swirl $\Delta V_{\theta gap}$ by over 75% compared with the reference configuration. This latter flow pattern is responsible for better inlet flow conditions at the tip of the blades which explain the enhanced values of torque and static efficiency for Config.4 as mentioned earlier in Table 5.
Config.3 exhibits a higher mass flow in the gap (+13%) compared with the reference configuration. This is a consequence of a higher pressure rise in the rotor observed for this optimum as mentioned earlier in Table 5. However, the swirl has been reduced by over 50% which enables to keep acceptable tip flow conditions and explains why the torque is not so deteriorated with respect to the higher static pressure difference and why the static efficiency remains at the same level as the one of the reference configuration.
These remarks have to be linked with the observation of Figure 11 where the mean meridian field of relative total pressure is represented for each configuration. The zone of low relative total pressure close to the tip ring (which is related with aerodynamic losses) is

reduced in both axial and radial directions for the two chosen optima compared to the reference configuration. Config.4 is the configuration which exhibits the most significant reduction of this zone.

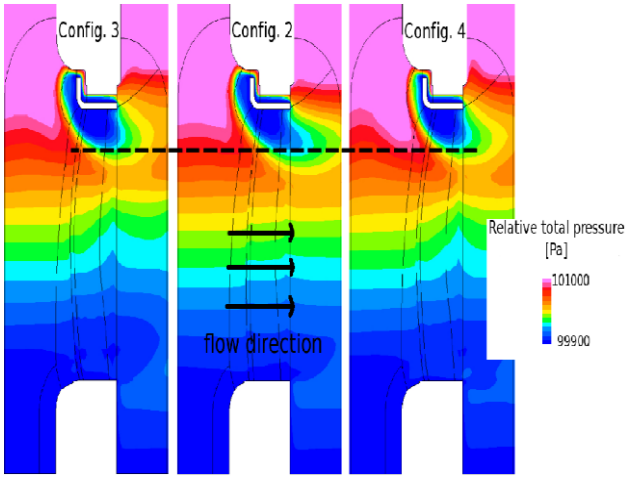

Fig. 11. Mean meridional field of relative total pressure

	ΔPs (Pa)	*τ* (N.m)	*η*
Config.2(Turb'Flow) 1ninth rotor, steady	192	0.501	0.626
Config.3 (Turb'Opty) 1 ninth rotor	214	0.533	0.630
Config.3 (Sc/Tetra) 1 ninth rotor, steady	233	0.636	0.625
Config.3 (Sc/Tetra) full rotor, steady	232	0.619	0.639
Config.3 (Sc/Tetra) full rotor, unsteady	243	0.623	0.625

Table 7. Comparison of overall performances

Even though Config.4 exhibits significant improvements regarding the torque and the static efficiency, a particular attention is payed on Config.3 as the main goal of this 3D blade re-adaptation is to increase the static pressure rise. Therefore, in order to confirm the extrapolated results, three additional CFD simulations are performed on Config.3 using the unstructured solver Sc/Tetra^{TM} [20][21]. These three flow simulations are carried out using a first-order implicit time scheme and a spatial upwind Monotone Upstream Centered Scheme for Conservation Laws (MUSCL) of second order. A k-omega Shear-Stress-Transport (SST) turbulence model [22][23] that has been shown to yield more accurate results on similar fans [1], is also used. An Arbitrary Lagrangian Eulerian method (ALE) [24][25] is chosen to rotate the mesh. The first flow simulation is steady and is performed on a one-ninth rotor geometry containing 5 million elements. The second one is also steady but is realized on a complete rotor geometry composed of 42 million elements.

The third one only differs from the second one by its unsteadiness. The first flow simulation is the most comparable to the extrapolated result. This simulation even provides a higher static pressure difference compared with the extrapolated one. As the torque does not grow unfavorably with respect to the growth of static pressure difference, the static efficiency is approximately the same as the one coming from the extrapolation. Static pressure difference and efficiency of the second and the third simulations are even better than the ones of the first simulation and than the extrapolated ones. These two last simulations enable to verify that both 360° flow structures and global unsteadiness level of the flow have a low influence on the criteria. All these results are presented in Table 7.

5 Conclusion

An optimization based on a high-order derivative database, produced by the Turb'Opty^{TM} parameterization code, has been applied to a 3D automotive shrouded fan with casing treatment. Contrary to other meta-modeling techniques, only a single CFD simulation is needed and extrapolation is used subsequently to create possible solutions. As the associated extrapolation tool is easily coupled to a multi-parameter multi-objective optimizer, a group of Pareto optimal solutions is found. In the present paper, two Pareto optimal fan configurations, chosen on the Pareto surface, are highlighted as they exhibit particularly interesting overall objective results. They show that the casing treatment coupled to re-designed blades can lead to significant enhancements.

Regarding the main objective, which is increasing the static pressure difference while

keeping acceptable value of the static efficiency compared to the reference configuration, Config.3 is the most promising optimum. The results of several flow simulations on this configuration show that the trend given by the derivatives is meaningful, which completely validates the use of this type of casing treatment.

Nevertheless, the static efficiency has not been increased compared with the reference configuration and this is probably because the casing treatment remains fixed in the present optimization. Indeed, the optimization of the casing treatment was performed separately from the fan. The next step of this study is to optimize simultaneously the fan and the casing treatment and the goal will be to maintain the level of static pressure difference obtained with Config.3 but also to increase the static efficiency. Thanks to the flexibility of the Turb'Opty^{TM} software, only the derivatives with respect to the grooving parameters will have to be computed and added to the actual derivative database. The future optimization will be based on this latter extended derivative database.

Acknowledgements

This work was part of CINEMAS^2 and ANR-TLOG07-011-03 LIBRAERO research programs. They were respectively funded by Région Rhône-Alpes / Lyon Urban Trucks and Bus (LUTB) and by the French National Agency of Research (ANR). Computations were performed at Centre Informatique National de l'Enseignement Supérieur (CINES).

References

[1] S. Moreau, M. Sanjosé, S. Magne, M. Henner. Aeroacoustic predictions of a low subsonic axial fan. *14th International Symposium on Transport Phenomena and Dynamics of Rotating Machinery Aeronautical Sciences*, ISROMAC-14, 2012.

[2] L. Soulat, S. Moreau, P. Ferrand, S. Aubert, M. Henner. Numerical design and optimization of a new casing treatment for shrouded fans. *27th International Congress of Aeronautical Sciences*, Nice, 2010.

[3] G. Vermes, A fluid mechanics approach to the labyrinth seal leakage problem. *ASME, Journal of Engineering for Power*, 83, 1961.

[4] S. M. Wellborn, I. Tolchinsky, T. H. Okiishi, Modeling shrouded fan stator cavity flows in axial flow compressors. *Journal of Turbomachinery*, 122, 2000.

[5] H. Zimmermann, K. H. Wolff, Air systems correlations, part 1: labyrinth seal. *Proceedings of ASME Turbo Expo*, Stockholm, 98-GT-206, 1998.

[6] A. M. Wallis, J. D. Denton, A. A. J. Demargne. The control of shroud leakage flow to reduce aerodynamic losses in a low aspect ratio, shrouded axial flow turbine. *Journal of Turbomachinery*, 123, 2001.

[7] V. Y. Nezym. Development of a new casing treatment configuration. *JMSE International Journal*, Series B, 47(4), pp. 804-812, 2004.

[8] I. Wilke, H. P. Kau. A numerical investigation of the influence of casing treatments on the tip leakage flow in a HPC front stage. *ASME Turbo Expo*, Amsterdam, 2002.

[9] S. Nadeau. Integral tip seal in a fan-shroud structure. *Siemens VDO Automative Inc.*, US Patent 56874900, 2005.

[10] R. W. Stairs, D. S. Greeley. High efficiency inflow-adapted axial flow fan. *Robert Bosch Corporation*, US Patent 6579063, 2003.

[11] M. Yapp, R. V. Van Houten and R. I. Hickey. Housing with recirculation control for banded axial flow fans. *Airflow Research and Manufacturing Corporation*, US Patent 5489186, 1996.

[12] D. C. Wisler, B. F. Beacher. Improved compressor performances using recessed clearances (trenches). *AIAA J. Prop.*, Vol. 5, pp. 469-475, 1989.

[13] J. Boudet, J. Caro, L. Shao and E. Lévêque. Numerical studies towards practical large-eddy simulation. *Journal of Thermal Science*, Vol. 16(4), pp. 328-336, 2007.

[14] J. C. Kok. Resolving the dependence of freestream values for the k-omega turbulence model. *AIAA Journal*, 38(7), 2000.

[15] S. Aubert, P. Ferrand, F. Pacull, M. Buisson. Fast CFD for shape and flow parameterization with metamodels built on high order derivatives, applications to fast design. *27th International Congress of the Aeronautical Sciences*, Nice, 2010.

[16] J. E. V. Peter and R. P. Dwight. Numerical sensitivity analysis for aerodynamic optimization: a survey of approaches. *Computers and Fluids*, Vol. 39, Issue 3, pp. 373-391, 2010.

[17] Y. Saad. Iterative methods for sparse linear systems. 2nd Edition. SIAM Publishing, Philadelphia, 2003.

[18] G. Gary Wang and S. Shan. Review of metamodeling techniques in support of engineering design optimization. *Journal of Mechanical Design*, Vol. 129, Issue 4, pp. 370-381, 2007.

[19] K. Deb, S. Agrawal, A. Pratap and T. Meyarivan. A fast elitist non-dominated sorting genetic algorithm

for multi-objective optimization: NSGA-2. *Report No. 200001, Indian Institute of Technology*, Kanpur, India.

[20] S. Tarumi et al.. The outline and the result of the ideas competition of the low drag car. *JSAE Symposium on Recent Activities in CFD towards Higher Quality*, No. 08-06, 2006.

[21] S. Sasaki, M. Fukuda, M. Tsujino and H. Tsubota. Prediction of aerodynamic noise in a ring fan based on wake characteristics. *Journal of Thermal Science*, Vol. 20, No. 2, 144-149.

[22] F. R. Menter. Zonal two-equation k-omega turbulence models for aerodynamic flows. *AIAA Paper* 93-2906.

[23] F. R. Menter. Two-equation eddy-viscosity turbulence models for engineering applications. *AIAA Journal*, Vol. 32, No. 8, pp. 1598-1605.

[24] C. W. Hirt, A. A. Amsden and J. L. Cook. An arbitrary Lagrangian Eulerian computing method for all flow speeds. *Journal of Computational Physics*, Vol. 14, pp. 227-253, 1974.

[25] R. K.-C. Chan. A generalized arbitrary Lagrangian Eulerian method for incompressible flows with sharp interfaces. *Journal of Computational Physics*, Vol. 17, pp. 311-331, 1975.

Copyright Statement